



Numerical study and enhancement of $\text{Ca}(\text{OH})_2/\text{CaO}$ dehydration process with porous channels embedded in reactors



Mengyi Wang, Li Chen^{*}, Pu He, Wen-Quan Tao

Key Laboratory of Thermo-Fluid Science and Engineering of MOE, School of Energy and Power Engineering, Xi'an Jiaotong University, Xi'an, Shaanxi, 710049, China

ARTICLE INFO

Article history:

Received 7 January 2019
 Received in revised form
 14 May 2019
 Accepted 26 May 2019
 Available online 27 May 2019

Keywords:

Thermochemical energy storage
 Dehydration
 Porous channel
 Enhanced reactive transport
 Numerical simulation

ABSTRACT

Thermochemical energy storage has drawn great attention due to its advantages such as high energy density, little heat loss, and long term and distance storage. The present study aims to enhance reactive transport processes during the dehydration process of $\text{Ca}(\text{OH})_2/\text{CaO}$. A physicochemical model is developed for the dehydration process occurring in porous reactant, including vapor flow, heat transfer and endothermic chemical reaction. Distributions of temperature and $\text{Ca}(\text{OH})_2$ concentration in cylinder reactors are discussed, and complicated coupling mechanisms are revealed between multiple processes. In addition, the results show that increasing temperature can efficiently enhance the reactive transport. Effects of reactant porosity are also explored and different reaction patterns are observed. Finally, porous channels with high thermal conductivity and permeability are embedded into the reactor. On the one hand, the porous channel with high permeability serves as highway for the vapor generated to be discharged out of the reactor, thus pushing the reaction towards dehydration direction. On the other hand, the porous channel with high thermal conductivity also enhances local heat transfer, thus accelerating the dehydration chemical reaction. In summary, with porous channels added, the dehydration process is greatly enhanced.

© 2019 Elsevier Ltd. All rights reserved.

1. Introduction

Due to the shortage of fossil energy, renewable energy has been widely adopted worldwide. However, renewable energy such as wind power and solar energy is limited by regional and seasonal factors, and its application is unstable and intermittent. To overcome such drawbacks, energy storage technology is adopted to provide continuous supply of energy as required. For storage and release of thermal energy, there are mainly three methods including explicit thermal storage, latent thermal storage and thermochemical energy storage. Explicit thermal storage conserves energy through sensible heat [1,2], while latent thermal storage (or phase change thermal storage) saves and releases thermal energy through phase transition of energy storage media [3,4]. Both these two methods require heat preservation device to preserve heat. Thermochemical energy storage is based on reversible chemical reactions to store and release energy. In the charging process, reactant absorbs heat and products are then preserved separately.

When heat is needed, products will be mixed at certain conditions to release heat. Compared with explicit and latent thermal storage, thermochemical energy storage has higher energy density, and can store energy at ambient temperature with little heat loss for a long time without heat preservation device [5,6], as long as reactants are well preserved separately. Thus, thermochemical energy storage can be adopted for long term preservation and long distance transportation of energy. However, compared with other two energy storage methods, the reaction system of thermochemical energy storage is usually more complex, and one-time investment of thermochemical energy storage device is higher. Even though, thermochemical energy storage is a great choice of high energy density and long term energy preservation.

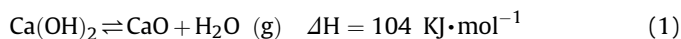
Thermochemical energy storage systems using different types of reactants have been proposed in the literature. For gas reactant systems, the decomposition of ammonia requires extremely high temperature to react [7,8]. Reaction temperature of methane reforming is lower than ammonia decomposition [9]. Both these two reactions require catalysts to accelerate reaction rate [10,11]. The separation and storage of gas reactants and products will bring up additional operation. The oxide/carbonate calcium system also

^{*} Corresponding author.

E-mail address: lichennht08@mail.xjtu.edu.cn (L. Chen).

Nomenclature		X	Reaction extent
A	Pre-exponential [s^{-1}]	<i>Greek symbols</i>	
c	Concentration [$\text{mol}\cdot\text{m}^{-3}$]	ϵ	Porosity of reactant
c_p	Heat capacity [$\text{J}\cdot\text{kg}^{-1}\cdot\text{K}^{-1}$]	ρ	Density [$\text{kg}\cdot\text{m}^{-3}$]
D	Diameter of reactor [m]	λ	Thermal conductivity [$\text{W}\cdot\text{m}^{-1}\cdot\text{K}^{-1}$]
D_p	Reactant particle diameter [m]	μ	Dynamic viscosity [$\text{Pa}\cdot\text{s}$]
E	Activation energy [$\text{J}\cdot\text{mol}^{-1}$]	<i>Subscripts</i>	
H	Height of reactor [m]	Ca(OH) ₂	Reactant Ca(OH) ₂
h	Characteristic length [m]	CaO	Product CaO
K	Reaction rate coefficient [s^{-1}]	eff	Effective
k	Permeability [m^2]	eq	Equilibrium
M	Mole mass [$\text{kg}\cdot\text{mol}^{-1}$]	solid	Solid reactant and product
p	Vapor partial pressure [Pa]	vapor	Product vapor
R_g	Mole gas constant [$\text{J}\cdot\text{mol}^{-1}\cdot\text{K}^{-1}$]		
T	Temperature of reactor [K]		

requires very high temperature for the charging process [12]. Decomposition of the oxide/carbonate lead system can start reaction at low temperature, but the energy density is low [13]. The metal/metal hydride system, such as Mg/MgH₂, produces hydrogen during discharge. The storage and use of hydrogen will bring in additional devices [14]. Decomposition of the oxide/hydroxide system is of medium-level temperature and relatively high energy density [15]. Reactants and products of this thermochemical system are solid powder and vapor. After the dehydration process, the solid product can be sealed, and the vapor can be collected by condensation or just directly discarded. Ca(OH)₂/CaO is one of the oxide/hydroxide reactants, which has several advantages such as high safety, non-toxic, low cost and high energy density [12]. Thus it is the topic of the present study. The dehydration/hydration processes of Ca(OH)₂/CaO is described by the following reversible reaction



During the dehydration process, reactant Ca(OH)₂ is heated to a temperature higher than the equilibrium temperature at corresponding pressure to decompose, during which heat is absorbed and vapor is generated.

There are mainly three types of reactors for Ca(OH)₂/CaO system including indirect-type, direct-type and continuous reactor [16]. In indirect-type reactor, also called packed bed reactor, reactant is packed inside the reactor without direct contact with heat transfer fluid and the outside atmosphere. A 10 kW packed bed reactor with oblate cubic reactor was experimentally studied by Schmidt et al. [17]. The reactor consisted of ten reaction units with channels between two units, through which heat transfer fluid flowed. Different levels of thermal power were acquired by adjusting the flow rate of heat transfer fluid. Vapor pressure (1.4 kPa–470 kPa) and temperature (280 °C–600 °C) in wider range were investigated with modified reactors in Refs. [18,19]. It was found that reaction rate at low pressure was limited, while when pressure was over 200 kPa, reaction would take place even at equilibrium temperature. Based on the above experimental studies, a model for the hydration/dehydration processes in an oblate cubic reactor was established by Ranjha and Oztekin [5]. The dehydration and hydration processes in a cylindrical reactor were investigated experimentally by Yan and Zhao [20]. It was found that higher wall temperature could effectively shorten the reaction time.

For direct-type reactor, the heat transfer fluid and vapor directly flow through and react with reactant powder. Based on experimental results of a cylindrical reactor [21], a two dimensional

model was developed by Schaubé et al. [22]. It was observed that the vapor partial pressure had little impact on reaction rate. It was also found that the state of reaction was still steady after 25 re-cycles, but the diameter of the reactant particles increased. The hydration process in a direct-type reactor was numerically simulated by Deng et al. [23]. It was found that during the hydration process, a district of high reaction rate was observed moving from inlet to outlet. Effects of vapor pressure and heat transfer gas flow rate on reaction rate were also studied. When the vapor partial pressure was increased from 0.5 to 1 bar, the reaction exothermic power increased from 80 to 110 kW. However, when the vapor partial pressure was increased continuously, growth of reaction exothermic was very small, indicating that vapor partial pressure can merely affect the reaction power in a certain range.

Finally, for the continuous reactor, the energy saving and release processes proceed without intermittence by importing reactant and exhausting product continually. This is always achieved by the fluid bed reactor. A reaction system based on circulating fluidized bed was designed and improved by Criado et al. [24,25]. The hydration and dehydration processes were studied experimentally. Vapor and solid reactant were fed into the reactor at certain temperature and pressure to release or store energy. Products left the reactor when reaction is finished, driven by flow of extra vapor and air. Based on experimental results, a standard bubbling fluid reactor model was established and then validated. Al₂O₃ was mixed with reactant by Pardo et al. [26] in a fluidized bed reactor to facilitate the flow of reactant particles.

Currently, the reaction kinetics, the transport processes and the stability of Ca(OH)₂/CaO systems still need to be further improved. Reaction cycles of CaO/Ca-silicates reactant were experimentally studied by Criado et al. [27]. It was found that better mechanical stability was acquired by improving the synthesis of the material. In another study, pure CaO reactant was mixed with natural limestone by Sakellariou et al. [28]. The reaction system was of well structural stability with 50% hydration extent, indicating that it was suitable for long-term operation. In addition, to avoid agglomeration of reactant and to improve the stability of circulation, reactant was encapsulated into porous ceramic shells by Afflerbach et al. [29]. Besides, catalysts were also added into the system to accelerate the reactions. Reactant Ca(OH)₂ was doped with Li(OH)₂ by Yan and Zhao [30] to accelerate the energy storage process. A new kinetic equation of dehydration and hydration was proposed based on experimental results which matched the experimental results very well.

From above review, it can be concluded that the reactive

transport process inside the reactor should be further enhanced to achieve faster and more efficient dehydration/hydration processes of Ca(OH)₂/CaO system. However, to the best of our knowledge, optimization of the inner structures of the reactor to enhance the reactive transport process is rare in the literature. In the present study, a physicochemical model of dehydration process for Ca(OH)₂/CaO system is established, including heat transfer, fluid flow and chemical reaction. The reactive transport processes during the dehydration process are discussed in detail. Emphases are placed on fluid flow, heat transfer and evolution of Ca(OH)₂ concentration. Then, effects of outlet pressure, side wall temperature and porosity on the dehydration processes are explored. Based on above studies, porous channels with higher thermal conductivity and permeability are embedded into the reactor, which is proved to facilitate vapor drainage and improve heat transfer process.

2. Physicochemical model

The dehydration process is studied in an indirect-type cylinder reactor as shown in Fig. 1. The diameter *D* and height *H* of the cylinder reactor are 100 and 800 mm, respectively. According to previous studies [5,16,17] the left surface of the reactor is sealed bottom surface and the right surface is outlet for vapor. To better understand the heat and mass transport inside the reactor, six observation points are selected on the profile *x* = 0. The coordinates of the six observation points are shown in Fig. 1. Initially, the reactor is filled with Ca(OH)₂ powder. To establish the physicochemical model, the following assumptions are adopted:

- (1) The equilibrium thermal model for heat transfer in porous media is adopted, indicating that the solid reactant and vapor are in thermal equilibrium.
- (2) The particle diameter and porosity of reactant do not change as reaction proceeds.
- (3) The thermal conductivity of Ca(OH)₂ and CaO do not change with temperature.
- (4) The vapor is treated as ideal gas.
- (5) Only dehydration process is studied while hydration process is the topic of future studies.
- (6) The thermal resistance between the reactant particles, the porous channel, and the side wall of the reactor is ignored.

2.1. Chemical reaction

The relationship between the equilibrium temperature and pressure of the dehydration process has been investigated experimentally in the literature. The following equilibrium equation proposed by Schaube et al. [31] is adopted in the present study

$$\ln\left(\frac{p}{100000}\right) = 16.508 - \frac{12845}{T_{eq}} \quad (2)$$

Eq. (2) is plotted in Fig. 2. When temperature is over the equilibrium temperature *T*_{eq} at related pressure, the reaction proceeds towards the positive direction and the endothermic dehydration happens. Once the temperature is below the equilibrium temperature, the dehydration will stop and exothermic hydration starts. Hence, to ensure launch of the dehydration, the initial temperature of simulation should be set over or equal to the equilibrium temperature related to the initial pressure. Besides, it is obvious that higher pressure asks for higher equilibrium temperature. In practice, it is hard to achieve excessively high temperature. Low pressure can be achieved much more easily. Thus in experimental researches, the initial pressure of dehydration is always set at relatively low level by vacuum pump [18–20].

During the dehydration process, the reactant Ca(OH)₂ is consumed, meanwhile CaO and vapor are generated in the same mole amount. The reaction rate can be calculated as follows

$$\frac{\partial c_{Ca(OH)_2}}{\partial t} = -K \cdot c_{Ca(OH)_2}$$

$$\frac{\partial c_{CaO}}{\partial t} = -K \cdot c_{CaO} \quad (3)$$

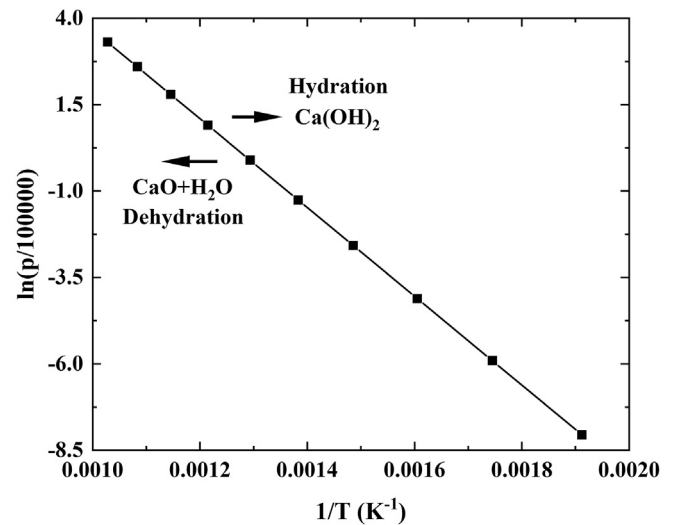


Fig. 2. Relationship between equilibrium temperature and equilibrium pressure.

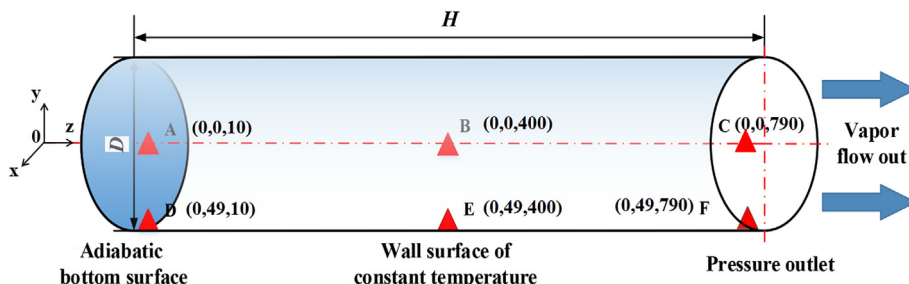


Fig. 1. Schematic of the cylinder reactor: the boundary condition and the six observation points on the profile *x* = 0.

$$\frac{\partial c_{\text{vapor}}}{\partial t} = K \cdot c_{\text{Ca(OH)}_2}$$

where $c_{\text{Ca(OH)}_2}$, c_{CaO} , c_{vapor} are mole concentrations of Ca(OH)_2 , CaO and vapor respectively.

The reaction rate coefficient K is determined by the Arrhenius equation, and effect of pressure is also taken into account [5].

$$K = A \times \exp\left(-\frac{E}{R_g T}\right) \times \left(\frac{T}{T_{\text{eq}}} - 1\right) \quad (4)$$

where A is the pre-exponential factor of dehydration (or hydration), and E is the activation energy of dehydration (or hydration). Both the two parameters are constant for a certain reaction and can be obtained through experiments. In this article, the values in Ref. [31] are adopted, as listed in Table 1. From Eq. (2) it can be seen that the equilibrium temperature is function of the pressure. Thus the reaction rate coefficient K calculated in Eq. (4) is affected by both pressure and temperature. The reaction rate coefficient will increase when temperature raises or pressure decreases.

The initial value of reactant concentration is proportional to the porosity ε of reactant and is calculated by

$$c_{\text{Ca(OH)}_2, \text{ini}} = \frac{\rho_{\text{Ca(OH)}_2}}{M_{\text{Ca(OH)}_2}} \varepsilon \quad (5)$$

where $M_{\text{Ca(OH)}_2}$ is the mole mass of Ca(OH)_2 .

2.2. Conservation equations

The mass conservation equation of vapor is as follows

$$\frac{\partial(\varepsilon \rho_{\text{vapor}})}{\partial t} + \nabla(\rho_{\text{vapor}} \mathbf{u}) = Q_m \quad (6)$$

where \mathbf{u} is the superficial velocity of vapor. Q_m is the mass source term related to the dehydration reaction, and is calculated by

$$Q_m = M_{\text{vapor}} \cdot K c_{\text{Ca(OH)}_2} \quad (7)$$

where M_{vapor} is the mole mass of vapor.

The solid reactant can be treated as porous media consisting of tiny particles with diameter of about $5 \mu\text{m}$ [21]. It was found in experiments that after several reaction cycles, the reactant particles would aggregate together, but could be broken up easily. In the present study, the average diameter and the porosity of reactant particles are assumed to keep constant during the dehydration process. Vapor generated flows through the tiny reactant particles, and the momentum equation for vapor is

$$\frac{\partial(\rho_{\text{vapor}} \mathbf{u})}{\partial t} + \frac{\mathbf{u}}{\varepsilon} \cdot \nabla(\rho_{\text{vapor}} \mathbf{u}) = -\varepsilon \nabla p + \mu_{\text{vapor}} \nabla^2 \mathbf{u} + \mathbf{F} \quad (8)$$

and \mathbf{F} is the force term due to porous media

$$\mathbf{F} = -\frac{\mu_{\text{vapor}}}{k} \mathbf{u} \quad (9)$$

where k is the permeability calculated by Kozeny-Carman equation

$$k = \frac{D_p^2 \varepsilon^3}{180(1 - \varepsilon)^2} \quad (10)$$

where D_p is the average diameter of reactant particles. Because the vapor flows inside the porous reactant very slowly, the Forchheimer term standing for the inertial force is not considered in the force term.

Based on the local thermal equilibrium assumption, energy equation is as below

$$\frac{\partial((\rho c_p)_{\text{eff}} T)}{\partial t} + \nabla((\rho c_p)_{\text{vapor}} T) = -\nabla(\lambda_{\text{eff}} \nabla T) + S \quad (11)$$

the Source term in Eq. (11) caused by the endothermic reaction is calculated by

$$\dot{S} = -\Delta H \cdot K c_{\text{Ca(OH)}_2} \quad (12)$$

Taking porosity and different characteristics of Ca(OH)_2 and CaO into account, the effective physical parameters are defined as follows

$$(\rho c_p)_{\text{eff}} = \varepsilon (\rho c_p)_{\text{vapor}} + (1 - \varepsilon) (\rho c_p)_{\text{solid}} \quad (13)$$

$$\lambda_{\text{eff}} = \varepsilon \lambda_{\text{vapor}} + (1 - \varepsilon) \lambda_{\text{solid}} \quad (14)$$

Heat capacity and density of solid reactants change as reaction proceeds

$$c_{p, \text{solid}} = X c_{p, \text{CaO}} + (1 - X) c_{p, \text{Ca(OH)}_2} \quad (15)$$

$$\rho_{\text{solid}} = X \rho_{\text{CaO}} + (1 - X) \rho_{\text{Ca(OH)}_2} \quad (16)$$

where X is the fraction of the reactant that has been consumed, refers to the reaction extent

$$X = 1 - \frac{c_{\text{Ca(OH)}_2}}{c_{0, \text{Ca(OH)}_2}} \quad (17)$$

The specific heat capacities of CaO and Ca(OH)_2 change with temperature [5].

$$c_{p, \text{CaO}} = 0.1643 T + 799.15 \text{ J} \cdot \text{kg}^{-1} \cdot \text{K}^{-1} \quad (18)$$

$$c_{p, \text{Ca(OH)}_2} = 0.3829 T + 1218.87 \text{ J} \cdot \text{kg}^{-1} \cdot \text{K}^{-1} \quad (19)$$

The above fluid flow, heat transfer and chemical reaction processes during dehydration are simulated using COMSOL software. For the base case, the outlet surface is for vapor to flow out with pressure of 28415 Pa. The bottom surfaces is adiabatic wall, and the side wall surface is with constant temperature of 863 K. The initial temperature of reactor is 723 K and the initial pressure is the corresponding equilibrium pressure of 28415 Pa according to Eq. (2).

Table 1
Values of important variables in the simulations.

Symbol	Parameter	Value
M_{vapor}	Mole mass of vapor	0.018 kg mol ⁻¹
$M_{\text{Ca(OH)}_2}$	Mole mass of Ca(OH)_2	0.074 kg mol ⁻¹
D_p	Diameter of reactant	5 μm
ρ_{CaO}	Density of CaO	3320 kg m ⁻³
$\rho_{\text{Ca(OH)}_2}$	Density of Ca(OH)_2	2200 kg m ⁻³
λ_{solid}	Thermal conductivity of solid reactant	2 W m ⁻¹ K ⁻¹
A	Pre-exponential factor	$187 \times 10^7 \text{ s}^{-1}$
E	Activation energy	$187 \times 10^3 \text{ J mol}^{-1}$
ε	Porosity of reactant	0.8
T_{wall}	Wall temperature	863 K
p_{ini}	Initial pressure	28415 Pa
p_{out}	Outlet pressure	28415 Pa

The bulk density of reactant Ca(OH)_2 is $400\text{--}470\text{ kg m}^{-3}$, while the theoretical density of calcium hydroxide is 2200 kg m^{-3} [21]. Thus the porosity of reactant is around 0.78 to 0.81. Values of reactant porosity are usually set between 0.5 and 0.8 in the literature [5,23]. The porosity for the base case is set as 0.8, leading to initial Ca(OH)_2 concentration of 5945 mol m^{-3} according to Eq. (5). Values of other important variables are listed in Table 1.

To verify the grid independence, simulations with different number of grids are conducted including 26250, 52693, 140907, 265436 and 729840 for the base case. Fig. 3 shows the reaction time of cases with different amount of grids. Based on results in Fig. 3, grid number of 265436 is chosen for subsequent simulations.

3. Results and discussion

3.1. The base case

Fig. 4 displays the distribution and time-evolution of Ca(OH)_2 concentration of the base case. It can be observed in Fig. 4(a) that regions of low Ca(OH)_2 concentration expand from the side wall to the axial line, indicating that the dehydration reaction mainly proceeds from the side wall to the axial line. This is expected as heat flux is supplied from the side wall. Besides, due to lower local pressure, Ca(OH)_2 concentration in district near the outlet is relatively lower than the district inside the reactor. The time-evolution of Ca(OH)_2 concentrations at different observation points are further plotted in Fig. 4(b). It can be seen that Ca(OH)_2 concentration near the side wall (points D, E and F) decreases rapidly at the very beginning, indicating strong local chemical reaction. This is mainly due to the high heat flux from side wall. However, the concentration at the axial line (points A, B and C) requires much longer time to approach zero, due to low thermal conductivity of the solid reactant and inefficient heat supply. In addition, Ca(OH)_2 concentrations of points C and F near the outlet decrease faster than other points. Because the local pressure is low, thus the equilibrium temperature is low, leading to faster local reaction rate according to Eqs. (2) and (4).

Fig. 4(b) also shows the time-evolution of reaction extent (defined in Eq. (17)) for the base case. The accomplishment of the dehydration process requires 13400 s. It can be observed that the slope of X decreases as time proceeds, indicating the reaction gradually slows down. The first half of reaction extent costs around 3000 s, while the remaining half takes about 10400 s.

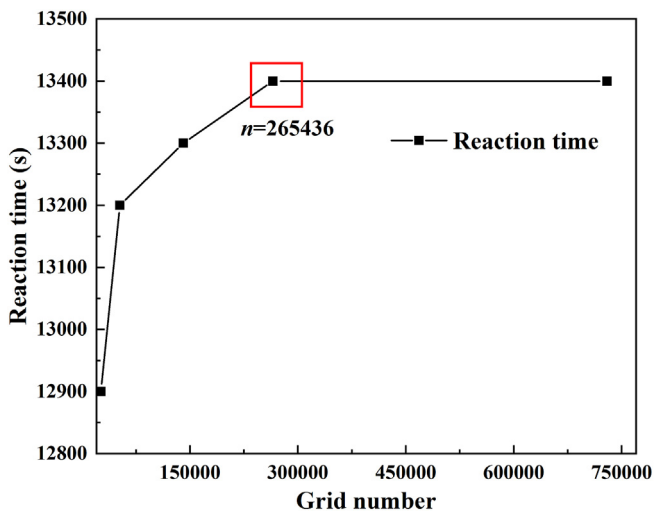


Fig. 3. Validation of grid independence.

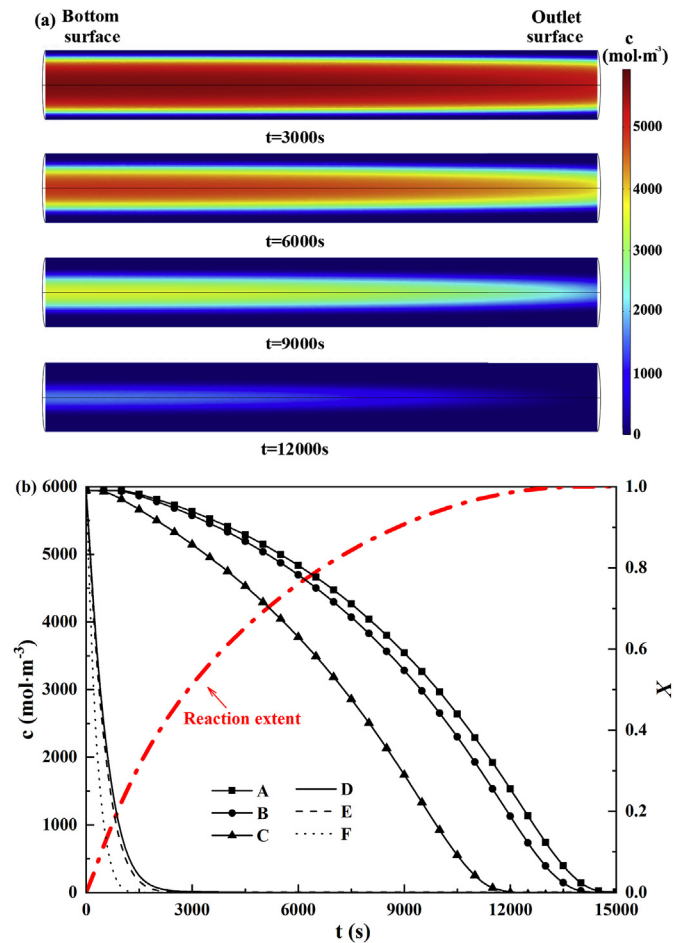


Fig. 4. Concentration for the base case. (a) Distribution of Ca(OH)_2 concentration on the profile $x = 0$ at different time; (b) time-evolution of Ca(OH)_2 concentrations of observation points and the volume average reaction extent.

Fig. 5 shows the temperature distribution and evolution of the base case. As shown in Fig. 5(a), the temperature near the side wall is higher than that inside the reactor, as expected. Correspondingly, the local reaction is stronger leading to lower local concentration, in agreement with the concentration field in Fig. 4(a). The time-evolution of temperatures of different observation points is shown in Fig. 5(b). Note that the endothermic reaction adsorbs heat, which will decrease the local temperature; while heat transfer from the side wall will increase the temperature. Hence, the temperature variation at a certain point actually is a combined result of the above two factors. As shown in Fig. 5(b), temperatures of near-wall points D, E and F raise rapidly in an extremely short time due to the short thermal conduction distance. Even though the fast reaction in points D, E and F leads to fast heat absorption, the high side wall temperature still can ensure fast reaction rate. As the temperature of points D, E, F increases near the side wall temperature, the difference between the wall temperature and local temperature is smaller. Therefore, the increase of the temperature slows down after the turning point in Box I.

The temperature variation of points A, B and C is also the result of competition of heat absorption and thermal conduction. The temperatures of these points increase slowly because of poor thermal conduction caused by the low thermal conductivity and the heat absorption. After the turning points in Box II at around 1300 s, the increase of temperature slows down and temperatures of A and B even decrease due to the endothermic reaction. Once the

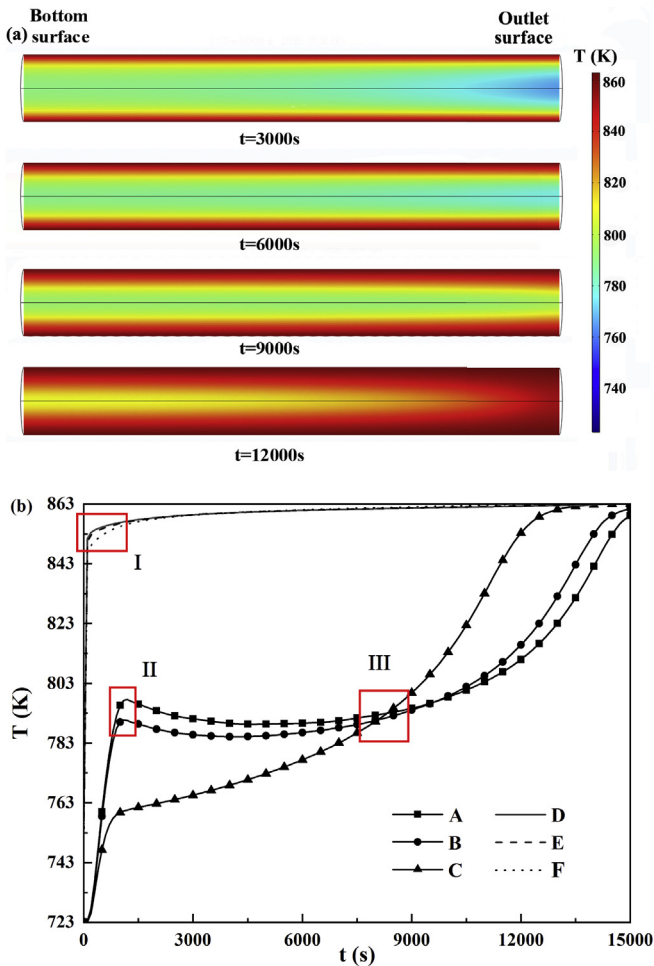


Fig. 5. Temperature of the base case. (a) Distribution of temperature on the profile $x = 0$ at different time; (b) time-evolutions of temperatures of observation points.

local temperature drops, the endothermic reaction rate slows down, leading to less heat absorbed and thus recovery of the temperature. When the thermal conduction and the heat absorption reach equilibrium, there will be a period of plateau temperature or slow increase after the turning points in Box II. As reaction proceeds, reaction rate slows down and thermal conduction is more than heat absorption. Thus after the turning points in Box III, temperatures of points A, B and C increase quickly again.

Now attention is turned to temperature variation of point C near the outlet. Before the intersection in Fig. 5(b) Box III, temperature of point C is lower than those of points A and B. From Fig. 4, it is found that reaction in point C is faster due to lower local pressure. This leads to more heat absorbed, and thus lower local temperature compared with points A and B. At the intersection point in Box III at around 8500 s, $\text{Ca}(\text{OH})_2$ concentrations of A, B and C are 3800, 3566 and 2135 mol m^{-3} respectively. According to Eq. (3), the reaction rate at point C will be lower than points A and B, leading to less heat absorption at point C according to Eq. (7). Thus, after the intersection in Box III, the temperature of point C is higher than points A and B.

A cylinder reactor with constant side wall temperature was experimentally studied by Yan and Zhao [20]. In their study, there were two observation points A at the axial line and B near side wall respectively, similar position with points C and F in the present study. The temperature variations in Ref. [20] and the present study

are similar. Thermochemical process in a cubic reactor was numerically studied by Ranjha et al. [5]. The heat transfer fluid flowed through the narrow channel between reactor without direct contact with reactant, and the vapor flowed out from reactor in perpendicular direction. Considering different types of reactor and boundary conditions, the evolution of temperatures of observation points here are qualitatively compared with results in Ref. [5]. In the present study, the temperature of points near side wall is higher than points at axial line, which is the same as Ref. [5]. Also in Ref. [5], after a while of fast increasing at the beginning, there is a period of plateau temperature, especially for points at axial line, which is similar with results in Fig. 5(a) here. In addition, the time evolution of reaction extent here is similar with that in Ref. [5].

3.2. Effects of outlet pressure and wall temperature

From above discussions, it can be found that pressure and temperature play important roles on the reactive transport process. In this section, the outlet pressure and the side wall temperature are changed to investigate their effects on reaction rate.

Firstly, the outlet pressure is changed to 20000 Pa, 15000 Pa and

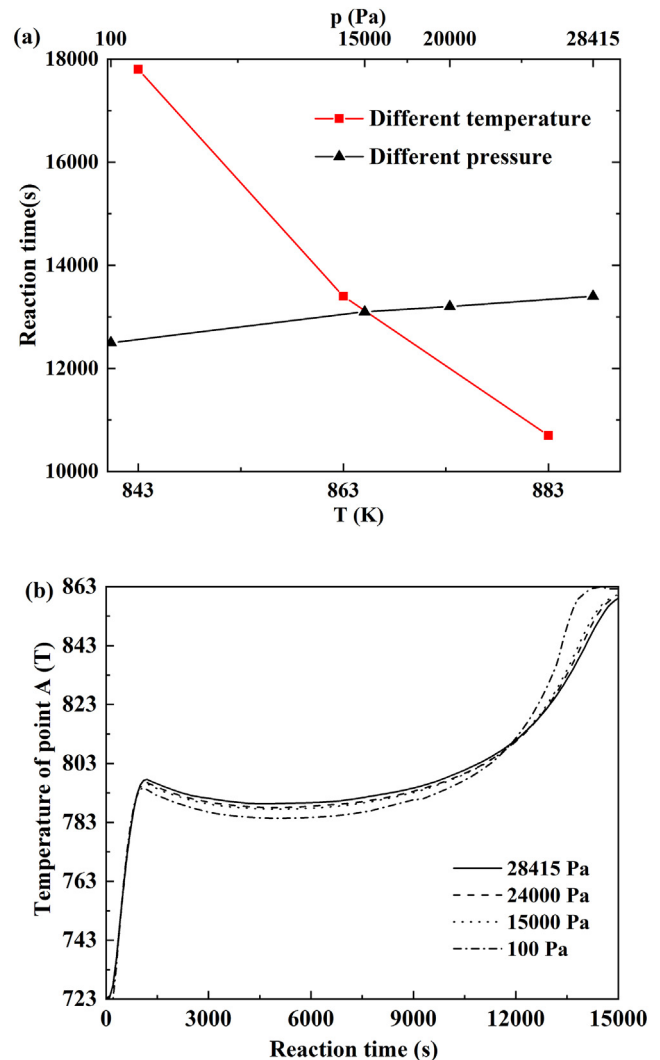


Fig. 6. Effects of boundary conditions. (a): Effects of wall temperature and outlet pressure on reaction time; (b): the temperature of point A of cases with different outlet pressures.

100 Pa respectively, while other parameters are the same with the base case. The three pressure values are lower than the corresponding equilibrium pressure (28415 Pa). As shown in Fig. 6(a), the pressure in the range studied has marginal effect on the reaction time. The reaction time for the case with outlet pressure of 100 Pa is only 6.7% less than the base case. By carefully examining the related temperature, $\text{Ca}(\text{OH})_2$ concentration and pressure field inside the reactor, it is found that the pressure drop from the bottom surface to the outlet changes little when outlet pressure is changed from 28415 Pa to 100 Pa. The outlet pressure merely has influence on regions quite close to the outlet, while most parts inside the reactor are still of high pressure because of vapor generated by the reaction. In the literature, the variation of vapor partial pressure also has little impact on reaction rate and reaction time [21]. Besides, the evolution of temperature of point A changes little when the outlet pressure varies from 28415 Pa to 100 Pa as shown in Fig. 6(b). Thus, the ratio of temperature and equilibrium temperature also changes little during the dehydration process. That means that effect of the outlet pressure on the reaction rate is weak.

Then the side wall temperature is changed to 843 K and 883 K with other parameters same with the base case. As shown in Fig. 6(a), the reactive transport process is very sensitive to the side wall temperature. Increasing the side wall temperature can effectively enhance the dehydration process. Reaction time of the case with side wall temperature of 883 K is around 19% less than the base case. In summary, in spite of the very low effective thermal conductivity of reactant, higher side wall temperature can significantly shorten the reaction time.

3.3. Effects of reactant porosity

In previous sections, the porosity of reactant is fixed at 0.8. In this section, the influence of porosity will be studied. The diameter of reactant particles is still $5\ \mu\text{m}$, and the initial and boundary conditions are same with the base case.

As shown in Fig. 7(a), the profile of the reactant concentration distribution with porosity of 0.4 is quite different from the results in Fig. 4(a) with porosity of 0.8. It can be seen that the reaction mainly advances from the outlet to the interior region, while in Fig. 4(b) it mainly proceeds from the side wall to the axial line. This is because with low porosity, the permeability of the reactant is also low, and thus the vapor generated is not easy to be removed out of the reactor, leading to the bullet shape of high concentration region in Fig. 7(a). Compared with results of the base case, the reaction is limited strictly inside the shell districts around the bullet shape. Correspondingly, movement of districts of low temperature and high reaction rate coefficient from the outlet to the bottom surface is also observed.

Reactant concentration and reaction time of cases with different porosities are further plotted in Fig. 7(b). The concentration of $\text{Ca}(\text{OH})_2$ increases proportionally as the porosity decreases, as expected. However, the reaction time increases more rapidly when the porosity decreases. For example, when the porosity is 0.4, the $\text{Ca}(\text{OH})_2$ concentration is 3 times of the base case, while the reaction time is around 6 times longer than the base case. On the one hand, lower porosity means higher reactant concentration and higher energy density. On the other hand, lower porosity causes higher pressure and slower reaction rate because more vapor is generated.

The pressure drops from the bottom surface to the outlet at different reaction extent with different porosities are shown in Fig. 7(c). As the outlet pressure is kept constant, the pressure drop also means the max pressure can be reached inside the reactor. As porosity decreases, the pressure drop rise up which means the

pressure inside the reactor also increases. Besides, the pressure drop reaches max value when reaction extent is 0.2 and then drops down. This is a result of competition between vapor generation and vapor flow. The temperature at different observation points for the case with porosity of 0.4 is shown in Fig. 7(d). Compared with temperature evolution in Fig. 5(b), the temperatures of points A, B and C increase to a higher level, and the plateau temperature period does not happen. This means that the slow reaction rate is mainly caused by high pressure inside the reactor rather than low temperature. The high pressure inside the reactor causes high equilibrium temperature, leading to lower reaction rate coefficient and slower reaction rate according to Eq. (4). In summary, in spite of the higher energy density related to the lower porosity case, the energy storage rate is greatly sacrificed, and effective discharge of the vapor generated is highly required.

3.4. Effects of porous channels embedded in the reactor

Based on the above simulations, it is found that enhancing the discharge of vapor is of great importance for accelerating the dehydration process. This inspires us to optimize the structures inside the reactor to promote the discharge of the vapor. In this section, for the first time, a porous channel is added into the reactor to study its effects on mass transport and the dehydration process. As schematically shown in Fig. 8, the porous channel is composed of two parts: a string of 11 porous disks and a porous slender cylinder throughout the disks along the axial line. The diameter and thickness of disks are 100 mm and 5 mm, and the gap between neighboring disks is 70 mm. The diameter of the slender cylinder is 10 mm. The outlets of the porous cylinder and reactor are in the same plane. There is no chemical reaction inside the porous channel. Permeability and thermal conductivity of the porous channel are set to be higher than that of the solid reactant to improve the heat and mass transport processes inside the reactor, and the results are presented as follows.

3.4.1. Effects of permeability of the porous channel

Note there is a maximum value for the permeability inside the porous channel, which is determined by the cubic law

$$k = \frac{1}{12}h^2 \quad (20)$$

where h is the characteristic length which is the thickness of disks here. Since h is 5 mm, the maximum permeability is $2.08 \times 10^{-6}\ \text{m}^2$.

The distributions of $\text{Ca}(\text{OH})_2$ concentration on the profile $x=0$ with porous channel of $2 \times 10^{-8}\ \text{m}^2$ permeability are shown in Fig. 9(a). The reactor is divided into small districts by the porous channel. Compared with results in Fig. 4(a), it can be found that local $\text{Ca}(\text{OH})_2$ concentration near the porous channel is relatively lower, as marked in the red box at 5000s. This is because the porous channel serves as highway for the vapor to flow out, and efficiently facilitates reaction towards the dehydration side, as schematically shown in Fig. 9(b). Besides, as shown in Fig. 9(c), the pressure is lower than the base case when a porous channel with $2 \times 10^{-8}\ \text{m}^2$ permeability is added. The pressure in the porous channel district is obviously lower than remaining districts. The porous channel indeed enhances the vapor flow. The promotion of vapor flow decreases the pressure inside the reactor, reducing the equilibrium temperature, and thus accelerating the reaction.

The relationship between reaction time and permeability of the porous channel in Fig. 9(d) confirms the reactive transport process is greatly enhanced by porous channel with higher permeability. Compared with the base case without porous channel, the mole

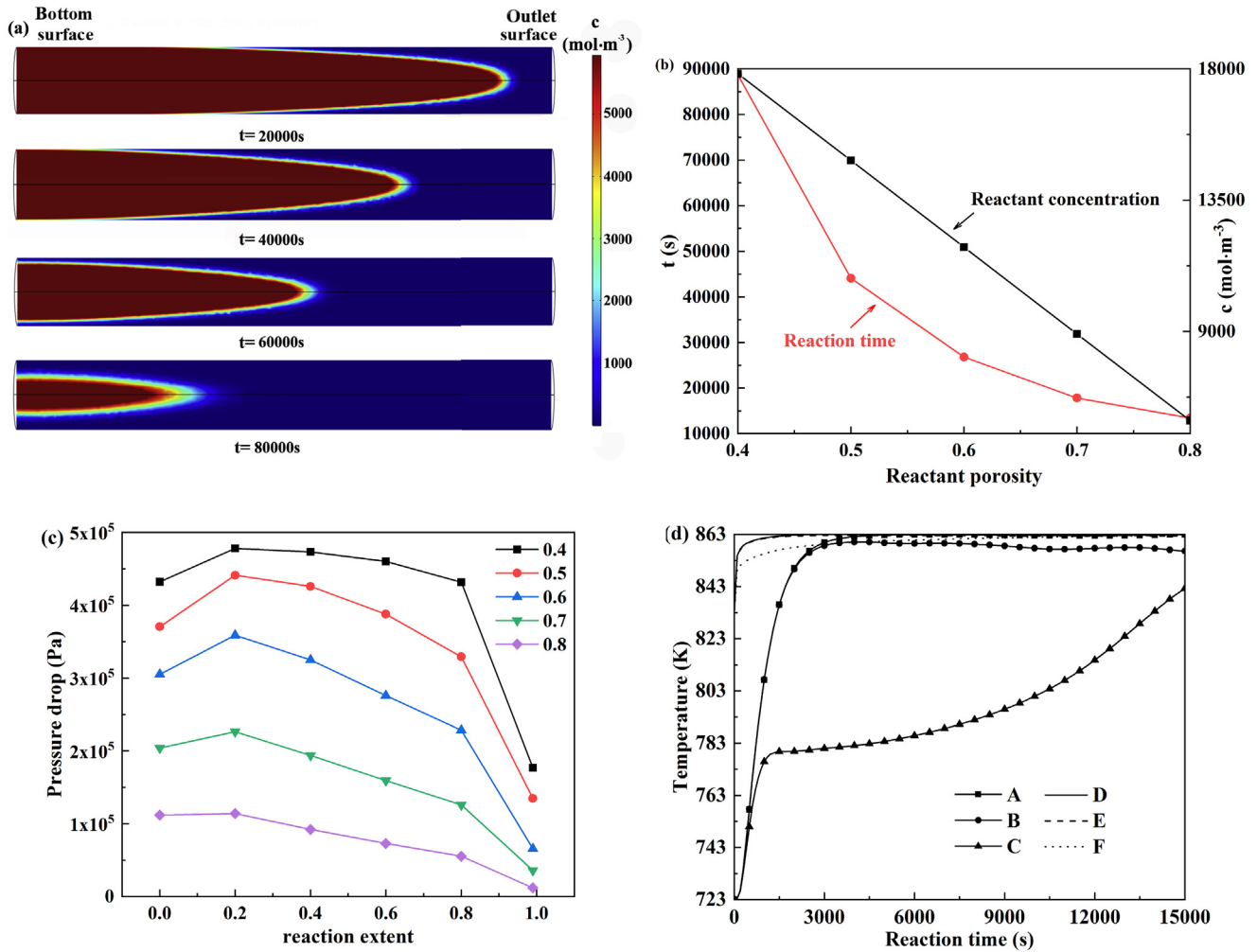


Fig. 7. Effects of porosity. (a) Distributions of $\text{Ca}(\text{OH})_2$ concentrations on the profile $x = 0$ at different time with porosity of 0.4; (b) reaction time and reactant concentrations for cases with different porosities; (c) pressure drop from bottom surface to outlet at different reaction extent with different porosities; (d) temperature evolution of observation points when porosity is 0.4.

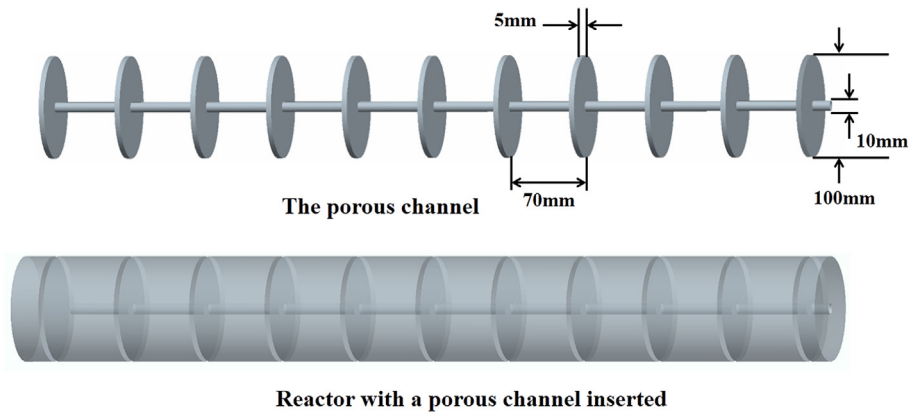


Fig. 8. Schematic of the reactor with a porous channel embedded.

amount of reactant of the case with the porous channel of $2 \times 10^{-8} \text{ m}^2$ permeability decreases by 7.77% while reaction time is greatly decreased by 22.39%. The slight sacrifice of the energy density is compensated by the faster reaction rate obtained.

3.4.2. Effects of thermal conductivity of the porous channel

Porous materials, such as metal foam, can be adopted to fabricate the porous channel shown in Fig. 8. The porous channel with higher thermal conductivity can greatly enhance the heat transfer inside the domain and thus can promote the dehydration process.

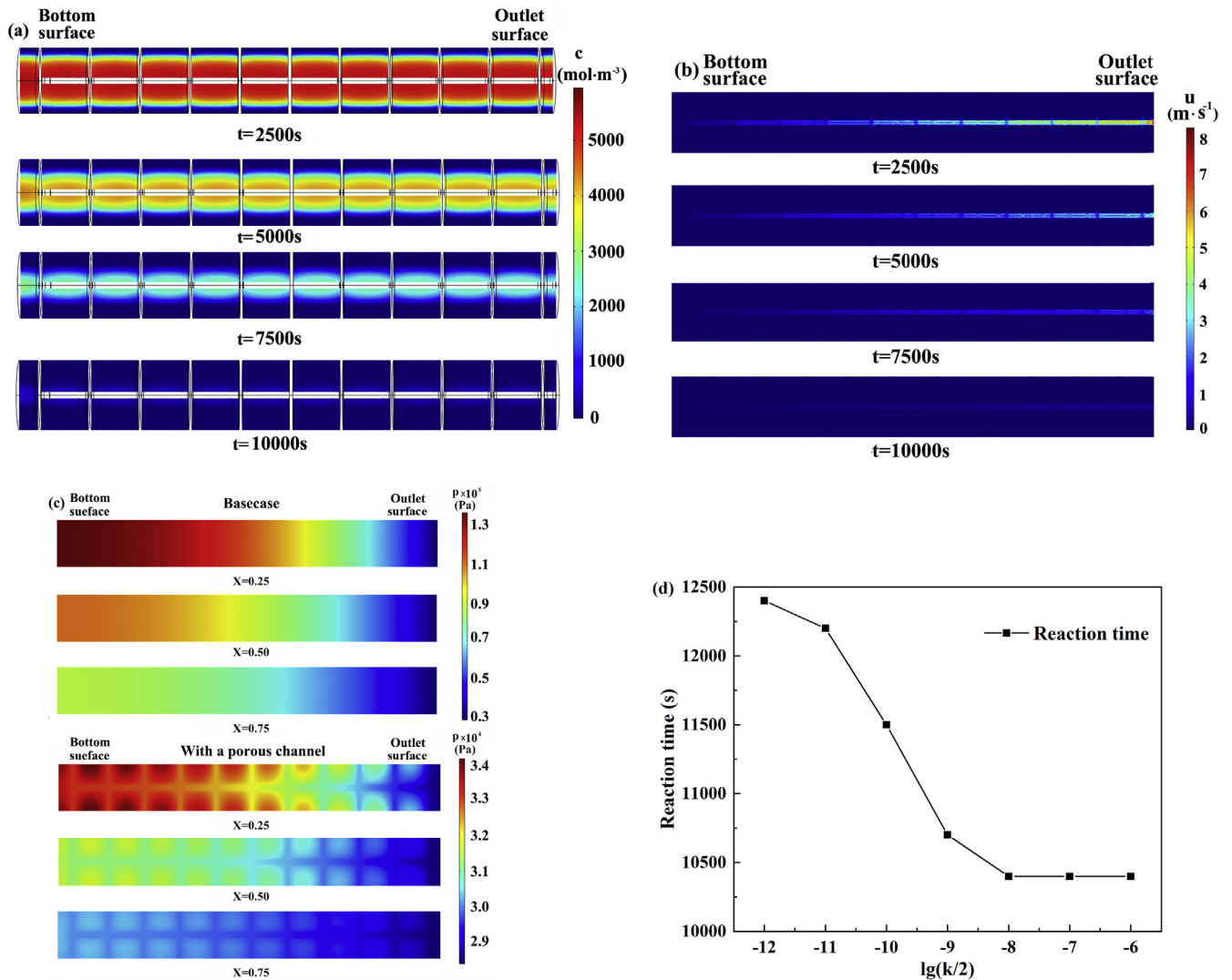


Fig. 9. Effects of permeability. (a) Distribution of Ca(OH)_2 concentration, (b) velocity on the profile $x=0$ at different moments with porous channel of $2 \times 10^{-8} \text{ m}^2$ permeability; (c) comparison of pressure on the profile $x=0$ between the base case and case with porous channel of $2 \times 10^{-8} \text{ m}^2$ permeability; (d) reaction time with porous channels of different permeabilities.

In this section, the thermal conductivity of solid frame of the porous channel is increased, leading to higher effective thermal conductivity of the porous channel according to Eq. (16). Fig. 10(a) and (b) show the Ca(OH)_2 concentration and temperature profile of the case with porous channel of $2 \times 10^{-8} \text{ m}^2$ permeability and $100 \text{ W m}^{-1} \text{ K}^{-1}$ solid frame thermal conductivity. Compared with Fig. 9, effects of the porous channel are more prominent.

It can be seen that thanks to the high thermal conductivity of the porous channel, heat transfers from the side wall to the interior of the domain along the porous disks, leading to higher local temperature as shown in Fig. 10(b). Compared with the base case, the reactant in each subdomain segmented by the porous channel is heated not only by the reactor side wall, but also by two neighboring porous disks. This certainly accelerates the dehydration process in the adjacent regions surrounding the porous channel, resulting in lower local concentration as shown in Fig. 10(a). Further, as discussed in Section 3.4.1, the porous channel of high permeability serves as highway to discharge the vapor generated, further facilitating the dehydration process. In summary, both heat transfer and fluid flow are enhanced by adopting the porous

channel with high permeability and thermal conductivity. The corresponding reaction time is plotted in Fig. 10(c). It can be seen that reaction time is effectively reduced by enhancing the heat transfer in the porous channel. For the case with permeability of $2 \times 10^{-8} \text{ m}^2$ and solid frame thermal conductivity of $400 \text{ W m}^{-1} \text{ K}^{-1}$, the reaction time is about 5800 s, 56.72% less than the base case of about 13400 s.

3.4.3. Effects of size of the porous channel

In this section, the diameter of the slender cylinder and thickness of the disks are changed to further study their effects on the dehydration process. The initial and boundary conditions are the same as the base case. The solid frame thermal conductivity of the porous channel is $400 \text{ W m}^{-1} \text{ K}^{-1}$, and permeability of the porous channel is $2 \times 10^{-8} \text{ m}^2$.

The thickness of the disks is changed from 5 mm to 8 mm and 10 mm, respectively, while diameter of cylinder keeps as 10 mm. Then diameter of the slender cylinder varies from 10 mm to 13 mm and 15 mm respectively with 5 mm disk thickness. Because the porous channel will decrease the amount of reactant, the energy

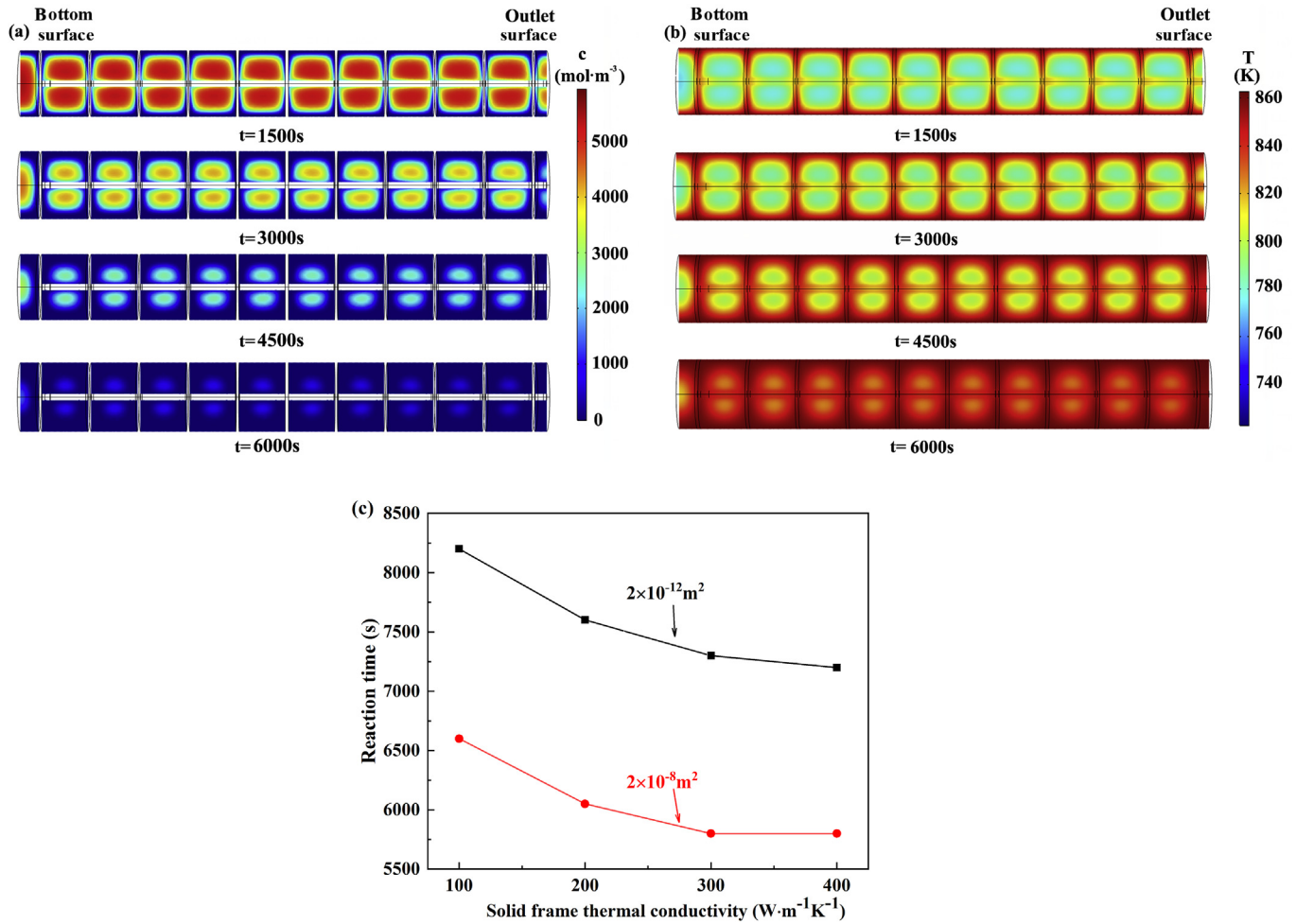


Fig. 10. Effects of solid frame thermal conductivity of the porous channel. (a) Ca(OH)_2 concentration and (b) temperature distribution on profile $x=0$ with the porous channel of $2 \times 10^{-8} \text{ m}^2$ permeability and $100 \text{ W m}^{-1} \text{ K}^{-1}$ thermal conductivity; (c) reaction time of porous channels with different permeabilities and solid frame thermal conductivities.

storage rate (ratio of amount of energy stored and reaction time) is employed for comparison. As shown in Fig. 11, the reaction time is the shortest for disk thickness as 10 mm, while the average energy

storage rate is highest when the diameter of the slender cylinder is 15 mm. The shortest reaction time does not mean highest energy storage rate.

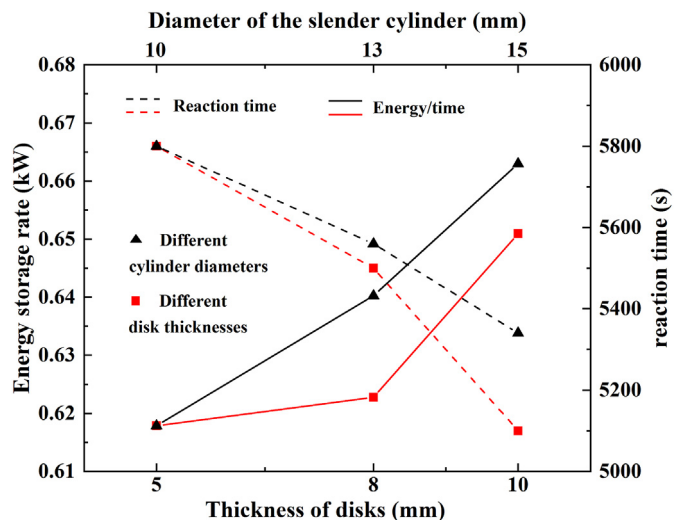


Fig. 11. Reaction time and energy storage rate of cases with porous channels of different sizes.

4. Conclusion

In the present study, the dehydration process of $\text{Ca(OH)}_2/\text{CaO}$ reversible reaction is numerically simulated. Distribution and time evolution of Ca(OH)_2 concentration, temperature, and reaction rate are discussed in detail. Complicated coupling mechanisms between different transport processes are revealed. The results qualitatively agree with previous experiments and simulations. Effects of side wall temperature and outlet pressure are investigated, and it is found that increasing the side wall temperature can efficiently accelerate the dehydration process. Effects of reactant porosity are also investigated, and it is found that changing the porosity leads to different reaction pattern. To improve the reactive transport process inside the reactor, porous channels are embedded into the reactor, and it is found that porous channels with higher permeability and thermal conductivity can efficiently enhance the heat transfer and facilitate the vapor discharge, thus accelerating the dehydration process.

Finally, effects of different factors on the hydration process are summarized in Fig. 12, where x axis shows different cases, while y axis denotes the reaction time in Fig. 12(a) and the energy storage rate in Fig. 12(b). The degree of enhancement of different factors on

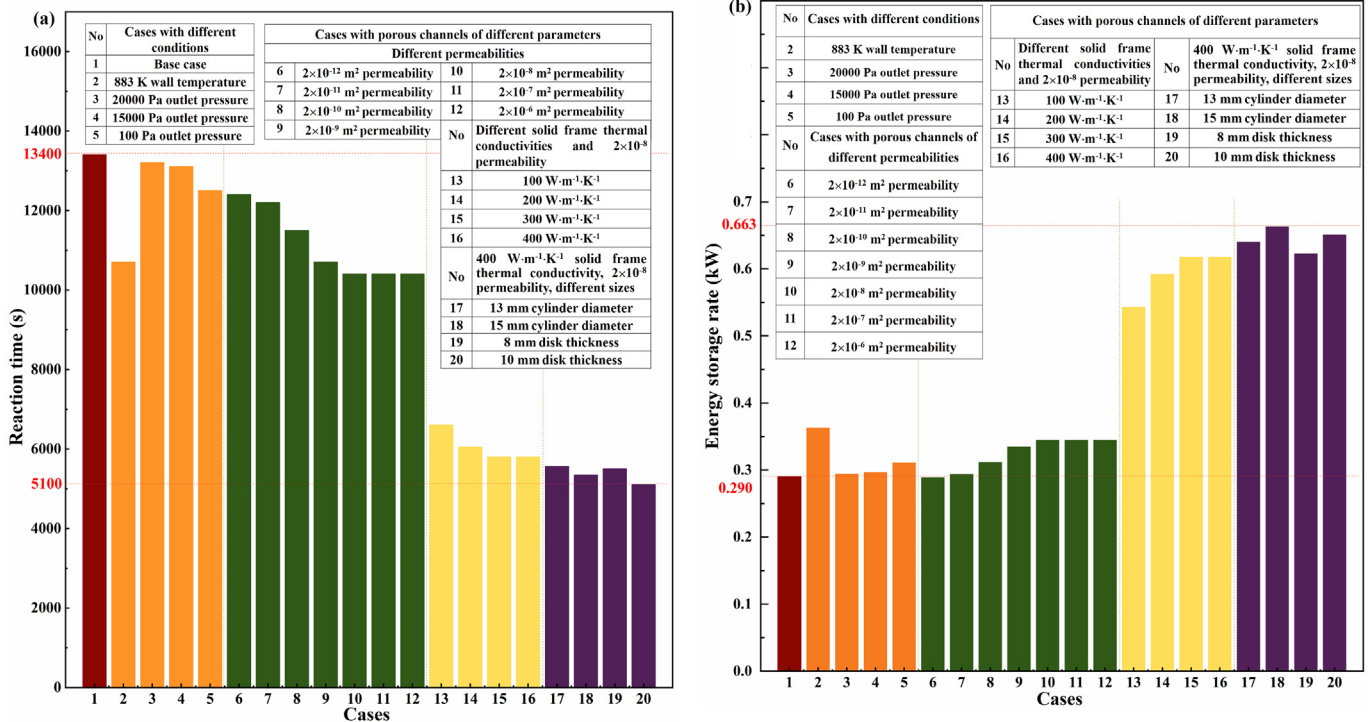


Fig. 12. Summary of effects of different factors on the dehydration process (a): Effects of different factors on the reaction time; (b): Effects of different factors on the energy storage rate.

reaction rate can be seen clearly. Higher side wall temperature, higher permeability, and higher solid frame thermal conductivity of the porous channels can reduce reaction time effectively. With the high thermal conductivity porous channel inserted, the reaction time is furtherly shortened, and energy storage rate reaches the maximum for case 18. Particularly, slow heat transfer inside the reactor is the limiting factor for dehydration process, and it is suggested to enhance the heat transfer inside the reactor, as clearly shown in Fig. 12.

Acknowledgement

This work was supported by the National Nature Science Foundation of China (51776159), Innovative Talents Support Plan of China Postdoctoral Foundation and the Fundamental Research Funds for the Central Universities. We also appreciate the two anonymous reviewers for their helpful comments, which greatly improve our work.

References

- [1] Mohan G, Venkataraman M, Gomez-Vidal J, Coventry J. Assessment of a novel ternary eutectic chloride salt for next generation high-temperature sensible heat storage. *Energy Convers Manag* 2018;167:156–64.
- [2] Lugolole R, Mawire A, Lentswe KA, Okello D, Nyeinga K. Thermal performance comparison of three sensible heat thermal energy storage systems during charging cycles. *Sustain Energy Technol Assess* 2018;30:37–51.
- [3] Lin Y, Alva G, Fang G. Review on thermal performances and applications of thermal energy storage systems with inorganic phase change materials. *Energy* 2018;165:685–708.
- [4] Liu J, Wang E, Zhao Y, Xu X, Moon J-S, Anantram MP. Impact of doping on bonding energy hierarchy and melting of phase change materials. *J Appl Phys* 2018;124(9):094503.
- [5] Ranjha Q, Oztekin A. Numerical analyses of three-dimensional fixed reaction bed for thermochemical energy storage. *Renew Energy* 2017;111:825–35.
- [6] Yadav D, Banerjee R. A review of solar thermochemical processes. *Renew Sustain Energy Rev* 2016;54:497–532.
- [7] Lovegrove K. Thermodynamic limits on the performance of a solar

- thermochemical energy storage system. *Int J Energy Res* 1993;17(9):817–29.
- [8] Lovegrove K. Exergetic optimization of a solar thermochemical energy-storage system subject to real constraints. *Int J Energy Res* 1993;17(9):831–45.
- [9] Kugeler K, Niessen HF, Röth-Kamat M, Böcker D, Rüter B, Theis KA. Transport of nuclear heat by means of chemical energy (nuclear long-distance energy). *Nucl Eng Des* 1975;34(1):65–72.
- [10] Fedders H, Harth R, Höhle B. Experiments for combining nuclear heat with the methane steam-reforming process. *Nucl Eng Des* 1975;34(1):119–27.
- [11] Fedders H, Höhle B. Operating a pilot plant circuit for energy transport with hydrogen-rich gas. *Int J Hydrogen Energy* 1982;7(10):793–800.
- [12] Pardo P, Deydier A, Anxionnaz-Minvielle Z, Rougé S, Cabassud M, Cognet P. A review on high temperature thermochemical heat energy storage. *Renew Sustain Energy Rev* 2014;32:591–610.
- [13] Kato Y, Saku D, Harada N, Yoshizawa Y. Utilization of high temperature heat from nuclear reactor using inorganic chemical heat pump. *Prog Nucl Energy* 1998;32(3):563–70.
- [14] Bogdanović B, Ritter A, Spliethoff B. Active MgH_2/Mg systems for reversible chemical energy storage. *Angew Chem Int Ed Engl* 1990;29(3):223–34.
- [15] Herrmann U, Kearney DW. Survey of thermal energy storage for parabolic trough power plants. *J Sol Energy Eng* 2002;124(2):145.
- [16] Pan ZH, Zhao CY. Gas–solid thermochemical heat storage reactors for high-temperature applications. *Energy* 2017;130:155–73.
- [17] Schmidt M, Szczukowski C, Roßkopf C, Linder M, Wörner A. Experimental results of a 10 kW high temperature thermochemical storage reactor based on calcium hydroxide. *Appl Therm Eng* 2014;62(2):553–9.
- [18] Schmidt M, Gutierrez A, Linder M. Thermochemical energy storage with $\text{CaO}/\text{Ca}(\text{OH})_2$ – experimental investigation of the thermal capability at low vapor pressures in a lab scale reactor. *Appl Energy* 2017;188:672–81.
- [19] Schmidt M, Linder M. Power generation based on the $\text{Ca}(\text{OH})_2/\text{CaO}$ thermochemical storage system – experimental investigation of discharge operation modes in lab scale and corresponding conceptual process design. *Appl Energy* 2017;203:594–607.
- [20] Yan J, Zhao CY. Experimental study of $\text{CaO}/\text{Ca}(\text{OH})_2$ in a fixed-bed reactor for thermochemical heat storage. *Appl Energy* 2016;175:277–84.
- [21] Schaub F, Kohzer A, Schütz J, Wörner A, Müller-Steinhagen H. De- and rehydration of $\text{Ca}(\text{OH})_2$ in a reactor with direct heat transfer for thermochemical heat storage. Part A: Experimental results. *Chem Eng Res Des* 2013;91(5):856–64.
- [22] Schaub F, Utz I, Wörner A, Müller-Steinhagen H. De- and rehydration of $\text{Ca}(\text{OH})_2$ in a reactor with direct heat transfer for thermochemical heat storage. Part B: Validation of model. *Chem Eng Res Des* 2013;91(5):865–73.
- [23] Deng C PZ, Yan J, Zhan CY. Numerical study on exothermic process of a $\text{CaO}-\text{Ca}(\text{OH})_2$ thermochemical heat storage system. *Energy Storage Sci Technol*. (7): 248–254.

- [24] Criado YA, Alonso M, Abanades JC, Anxionnaz-Minvielle Z. Conceptual process design of a CaO/Ca(OH)₂ thermochemical energy storage system using fluidized bed reactors. *Appl Therm Eng* 2014;73(1):1087–94.
- [25] Criado YA, Huille A, Rougé S, Abanades JC. Experimental investigation and model validation of a CaO/Ca(OH)₂ fluidized bed reactor for thermochemical energy storage applications. *Chem Eng J* 2017;313:1194–205.
- [26] Pardo P, Anxionnaz-Minvielle Z, Rougé S, Cognet P, Cabassud M. Ca(OH)₂/CaO reversible reaction in a fluidized bed reactor for thermochemical heat storage. *Sol Energy* 2014;107:605–16.
- [27] Criado YA, Alonso M, Abanades JC. Enhancement of a CaO/Ca(OH)₂ based material for thermochemical energy storage. *Sol Energy* 2016;135:800–9.
- [28] Sakellariou KG, Criado YA, Tsongidis NI, Karagiannakis G, Konstandopoulos AG. Multi-cyclic evaluation of composite CaO-based structured bodies for thermochemical heat storage via the CaO/Ca(OH)₂ reaction scheme. *Sol Energy* 2017;146:65–78.
- [29] Afflerbach S, Kappes M, Gipperich A, Trettin R, Krumm W. Semipermeable encapsulation of calcium hydroxide for thermochemical heat storage solutions. *Sol Energy* 2017;148:1–11.
- [30] Yan J, Zhao CY. Thermodynamic and kinetic study of the dehydration process of CaO/Ca(OH)₂ thermochemical heat storage system with Li doping. *Chem Eng Sci* 2015;138:86–92.
- [31] Schaub F, Koch L, Wörner A, Müller-Steinhagen H. A thermodynamic and kinetic study of the de- and rehydration of Ca(OH)₂ at high H₂O partial pressures for thermo-chemical heat storage. *Thermochim Acta* 2012;538: 9–20.